Eur. Phys. J. A **22**, 51–60 (2004)
DOI 10.1140/epja/i2004-10017-9

THE EUROPEAN PHYSICAL JOURNAL A

Possible explanation of fine structures in mass-energy distribution of fission fragments

A.V. Andreev[1], G.G. Adamian[1,2], N.V. Antonenko[1,a], S.P. Ivanova[1], and W. Scheid[3]

[1] Joint Institute for Nuclear Research, 141980 Dubna, Russia
[2] Institute of Nuclear Physics, Tashkent 702132, Uzbekistan
[3] Institut für Theoretische Physik der Justus-Liebig-Universität, D-35392 Giessen, Germany

Received: 24 March 2004 /
Published online: 12 October 2004 –
Communicated by V.V. Anisovich

Abstract. Within an improved scission point model, experimental data on the relative yield, mean value and variance of the total kinetic-energy distribution of fission fragments are described. It is shown that for a fixed mass and charge fragmentation, the potential energy of the scission configuration has several minima as a function of the deformation parameters of the fragments. The scission at these minima leads to a relatively enhanced yield of the fragments with a certain TKE and creates fine structures in the TKE-mass distribution which are different from those produced by the odd-even effect.

PACS. 24.75.+i General properties of fission – 21.60.Gx Cluster models

1 Introduction

A static analysis based on the potential energy surface is useful for describing various characteristics of fission. The mass, charge and kinetic-energy distributions of fission fragments are well described within the scission point model where a potential energy is calculated for a particular scission point configuration of two nearly touching coaxial nuclei [1]. Since ref. [1] was published, new experimental information [2–13] appeared on the mean total kinetic energy $\langle \mathrm{TKE} \rangle$ of the fission fragments as a function of their mass numbers. For example, the $\langle \mathrm{TKE} \rangle$ and its variance were measured for specific combinations of fission fragments in spontaneous fission of ^{252}Cf [9]. One of the interesting experimental data of the last years is the observation of fine structures in the TKE-mass distribution of fission fragments [14]. It was found that the TKE-mass distribution shows a smooth shape with small local peaks which are different from those produced by proton odd-even staggering. The method for revealing the fine structure is based on the difference between the original and smoothed experimental TKE-mass distributions. The first attempt to explain the fine structures was made in [15] within a cluster approach in which specific ruptures of a clustered neck create the peculiarities of the observed fine structures.

[a] e-mail: antonenk@thsun1.jinr.ru

In this paper we aim to describe new experimental fission data within an improved scission point model. As in ref. [1], we interpret the scission configuration as a dinuclear system (DNS) with the two fission fragments in contact. The DNS model has the advantage that the mass and charge asymmetries between the fragments are explicitly treated as collective degrees of freedom. A similar model was used in refs. [16,17] to derive the mass distribution in fission. Here, we want to explain the fine structures and total kinetic energies in fission in their dependence on the deformation of the fragments.

The potential energy of the DNS with fixed mass and charge numbers of the nuclei is calculated with respect to their deformation parameters in sect. 2. The proper calculation of the interaction between the fragments and of the deformation energies let us avoid the uncertainties in the choice of the internuclear distance and excitation energy in the scission configuration as it was the case in ref. [1]. The potential energy of the scission configuration as a function of deformations of the fragments has several minima. The scission at these minima produces local maxima in the TKE-mass distribution of fission fragments (sects. 3 and 4.1). We analyse in sect. 4.2 whether these maxima correlate with the observed fine structure in the neutron-induced fission $^{233}\mathrm{U}(n_{\mathrm{th}}, f)$. The calculated $\langle \mathrm{TKE} \rangle$ and variance of TKE in fission of ^{234,236}U, ^{240}Pu and ^{252}Cf, and the relative yields of fission fragments of ^{252}Cf are compared with the experimental data in sect. 4.3. A summary is given in sect. 5.

2 Potential energy of scission configuration

The fissioning nucleus with mass A and charge Z can be described at the scission point with the DNS model. Therefore, typical characteristics of the DNS as the excitation energy, the charge (Z_L, Z_H) and mass (A_L, A_H) numbers, and the deformation parameters (β_L, β_H) of light (L) and heavy (H) nuclei, respectively, determine the mass, charge and kinetic-energy distributions of the fission fragments. We treat the fragment pairs as nearly touching, coaxial prolate ellipsoids. The deformation parameters β_i are defined as the ratios of the semimajor (c_i) and semiminor (a_i) axes of the ellipsoids, $i = L$ or H. The volume conservation is taken into account. Since in the fission of actinides the saddle point configuration of the fission fragments corresponds to quite large deformations, the used shape parametrization is suitable up to $\beta_i \approx 2.1$. The quadrupole moment of an ellipsoid with $\beta = 2.1$ is equal to the quadrupole moment of a nucleus with a quadrupole deformation parameter of 0.65 if one uses the expansion of the nuclear surface in spherical functions.

Since we deal with a static description of fission, the crucial point of the model is the calculation of the potential energy. This energy is the sum of the liquid-drop $(U^i_{\rm LD})$ and microscopic shell correction $(\delta U^i_{\rm sh})$ energies for each DNS nucleus and the Coulomb $(V_{\rm C})$ and nuclear $(V_{\rm N})$ potential terms describing the interaction between the DNS nuclei,

$$\begin{aligned} U(\{A_i, Z_i, \beta_i\}, R, E^*) &= U^L_{\rm LD}(A_L, Z_L, \beta_L) \\ &+U^H_{\rm LD}(A_H, Z_H, \beta_H) + \delta U^L_{\rm sh}(A_L, Z_L, \beta_L, E^*) \\ &+\delta U^H_{\rm sh}(A_H, Z_H, \beta_H, E^*) + V_{\rm C}(\{A_i, Z_i, \beta_i\}, R) \\ &+V_{\rm N}(\{A_i, Z_i, \beta_i\}, R). \end{aligned} \quad (1)$$

Here, $A_H = A - A_L$, $Z_H = Z - Z_L$, and E^* is the excitation energy of the pre-scission configuration. The Coulomb potential $V_{\rm C}$ is calculated with the method given in ref. [18]. The calculation of $V_{\rm N}$ is done in the double-folding form described in ref. [19]. The decaying DNS starting at the touching distance $R_m \approx c_L + c_H + 0.5$ fm has to overcome a small potential barrier $\Delta V = U(R_b) - U(R_m)$ at $R_b \approx c_L + c_H + 1.5$ fm [19,20] which results from the sum of the attractive nuclear and repulsive Coulomb potentials. This barrier keeps the DNS nuclei in contact for some time and allows the DNS nuclei to take statistical distributions in the space (β_L, β_H). The value of ΔV in the considered DNS is less than 3 MeV and depends on the mass (charge) splitting in fission and on the deformations of the fragments. Since with the used shape parametrization of the DNS nuclei the value of ΔV becomes very small at large deformations of the nuclei, we restrict our treatment to that intervals of β_L and β_H where $\Delta V > 0$. Indeed, configurations without a potential barrier, which prevents the immediate DNS decay, play no role because the DNS decays with large probability before reaching this configuration. We do not consider β_L and β_H larger than 2.1 since the development of very large deformations needs time for which the statistical assumptions used in this paper are not valid. It is necessary to stress that in comparison to ref. [1] our model allows us to define the internuclear distance strictly in the scission configuration.

2.1 Liquid-drop energy with variable surface tension

The liquid-drop energy and shell corrections are calculated with the two-center shell model [21] the parameters of which are chosen to have the best fit of the experimental binding energies of the separate nuclei. We modified the calculation with the two-center shell model by a deformation-dependent surface tension and separately calculated the energy of each fragment. The liquid-drop energy $U^i_{\rm LD} = E^i_{\rm C} + E^i_{\rm s}$ $(i = L$ or $H)$ of the nucleus "i" consists of the Coulomb $E^i_{\rm C}$ and surface energy $E^i_{\rm s}$ terms. The last one is proportional to the area S^i of nuclear surface

$$E^i_{\rm s} = \sigma_i S^i \,, \quad (2)$$

where σ_i is the surface tension coefficient. With a constant surface tension $\sigma_i = \sigma_{0i}$ the calculated moment of inertia of a fissioning nucleus is larger than the experimental one. This indicates a smaller deformation of the real nucleus at the saddle point than one obtains with a constant σ_{0i} [22,23]. To avoid this drawback, we propose to use a deformation-dependent $\sigma_i(\beta)$ in contrast to the procedure done in the model of ref. [1]. This effectively takes the change of the nuclear surface with deformation into account. The corrections to the surface energy which arise from the change of the curvature of the surface and from effects caused by the finite compressibility of nuclear matter were treated in the droplet model [22]. These effects are automatically included in the model if finite-range nuclear forces are used for calculating $E_{\rm s}$ [24].

In order to remain within the liquid-drop model, we introduce a dependence of σ_i on β in a simple way,

$$\sigma_i(\beta) = \sigma_{0i}(1 + k_i(\beta - \beta^{\rm gs})^2) \,, \quad (3)$$

where $\sigma_{0i} = 0.9517(1–1.7826((N_i - Z_i)/A_i)^2)$ as in ref. [21] with $N_i = A_i - Z_i$. Thus, near the ground state with the deformation $\beta^{\rm gs}$ the parameters of the usual liquid-drop model are not changed. However, for large deformations the surface tension increases if $k_i > 0$. The value $k_i = 0.002$ corresponds to the value $\Gamma = -0.1$ suggested in ref. [23] to take the deformation of a diffuse matter layer around the nucleus into account. However, with $k_i = 0.002$ a DNS consisting of magic nuclei would have unrealistically large deformation at the scission point which yields a too small TKE in comparison with the experiment. In contrast to non-magic nuclei, the deviation of magic nuclei in the deformation from their ground states creates larger changes in the shell structure and, thus, in the diffuseness. A large increase of the diffuseness with deformation in magic nuclei leads to a sharp decrease of the binding energy. The influence of this effect can be taken care of by using a larger $k_i = (0.01–0.05)$ for magic nuclei. Therefore, we propose to insert in (3)

$$k_i = \frac{0.06}{1 + \exp[-0.063(C_{\rm vib}(Z_i, N_i) - 67)]} \,, \quad (4)$$

where $C_{\rm vib}$ is the stiffness of the nucleus with respect to the quadrupole deformation. Large $C_{\rm vib}$ for magic nuclei results in larger values of k_i. The stiffness parameter is determined as [25]

$$C_{\rm vib}(Z_i, N_i) = \frac{\hbar\omega^i_{\rm vib}(3Z_iR^2_{0i}/(4\pi))^2}{2B(E2)^i_{\rm vib}}\,, \qquad (5)$$

where $R_{0i} = 1.15A_i^{1/3}$ fm and $B(E2)^i_{\rm vib} \approx E^i_{2^+}B(E2)^i_{\rm rot}/(\hbar\omega^i_{\rm vib})$. Since not in all nuclei the first 2^+ state is of vibrational nature, we assume the 2^+ states presented in [26] as vibrational ones if $B(E2)^i < 0.55\,e^2{\rm b}^2$. If $B(E2)^i \geq 0.55\,e^2{\rm b}^2$, the 2^+ states given in ref. [26] are considered as rotational ones. In this case the vibration energy can be estimated as $\hbar\omega^i_{\rm vib} = E^i_{2^+}B(E2)^i/0.55$ with $E^i_{2^+}$ as the energy of the first 2^+ state. For known vibrational states in nuclei with $\hbar\omega^i_{\rm vib} > E^i_{2^+}$, this estimation is quite good.

With (4) the constants k_i deviate much from 0.002 only for nearly magic nuclei and allow us to avoid the shift of the minima of the DNS potential energy to large deformations of these nuclei. Thus, values of $k_i = (0.01$–$0.05)$ are suitable for such magic or nearly magic nuclei like ^{126,130,132}Sn, ^{132,134,136}Te and ^{138,140}Xe which occur in the DNS considered in this paper. These values change the values of σ_i with respect to σ_{0i} less than 0.25% for the deformations corresponding to the minima of the potential energy of the scission configuration as a function of β_L and β_H. For non-magic nuclei, the change of σ_i with β is negligible.

2.2 Shell corrections

With the two-center shell model [21] one can obtain the microscopic shell correction $\delta U_{\rm sh} = \delta U^L_{\rm sh} + \delta U^H_{\rm sh}$ for the dinuclear system at zero excitation energy. This model allows us to find the shell correction $\delta U^i_{\rm sh}$ for separate fragment as well when we consider the DNS consisting of two identical nuclei, $\delta U^i_{\rm sh} = \delta U_{\rm sh}/2$. We found that the difference between $\delta U_{\rm sh}$ obtained by two methods does not exceed 1 MeV that is within the inaccuracy of our calculation. Note that the present calculations are justified for the range $\beta < 2.1$ which is suitable for the used shape parametrization.

The calculated $\delta U^i_{\rm sh}(A_i, Z_i, \beta_i, E^* = 0)$ are in good agreement with the results presented in refs. [24,27]. Figure 1 shows the quantities $E_{\rm C}$, $E_{\rm s}$, $\delta U^i_{\rm sh}$ and U as functions of the deformation parameter at $E^* = 0$ MeV for ^{102}Zr, ^{108}Mo and ^{132}Sn. At the deepest minima of U the deformations of the nuclei are consistent with the quadrupole moments following from the calculations [24] or from the experiment [26]. For ^{102}Zr, refs. [24] and [27] give $\delta U_{\rm sh} = 1.89$ and 3.2 MeV, $\beta = 1.36$ and 1.37, respectively. For ^{108}Mo, refs. [24] and [27] give $\delta U_{\rm sh} = 2.01$ and 3.71 MeV, $\beta = 1.33$ and 1.33, respectively. For ^{132}Sn, refs. [24,27] give $\delta U_{\rm sh} = -12.61$ and -11.55 MeV, respectively. Reference [26] gives only the values $\beta = 1.43$, 1.38 and 1 for the nuclei ^{102}Zr, ^{108}Mo and ^{132}Sn, respectively.

The odd multipoles are not included in our calculations. While in ref. [24] only even multipoles were considered, the octupole deformations were incorporated in ref. [27]. For the nuclei presented in fig. 1, $\beta_3 = 0$ in accordance with ref. [27]. For ^{146}Ba in the ground state, ref. [27] predicts $\beta = 1.199$ (in our notation), $\beta_3 = -0.107$ and $\delta U_{\rm sh} = -0.02$ MeV, ref. [24] predicts $\beta = 1.19$ and $\delta U_{\rm sh} = -0.72$ MeV, and the experiment gives $\beta = 1.22$ [26]. Our calculation leads to $\delta U_{\rm sh} = -1.3$ MeV and $\beta = 1.22$ that allows us to conclude about good agreement of our results with the calculations of ref. [27] even in the case of $\beta_3 \neq 0$ in [27]. With the account of β_3 the quadrupole deformation in the ground state is slightly different from the one obtained in the case of $\beta_3 = 0$. The octupole deformation changes $\delta U_{\rm sh}$ within 1–1.3 MeV that is quite small for our purposes.

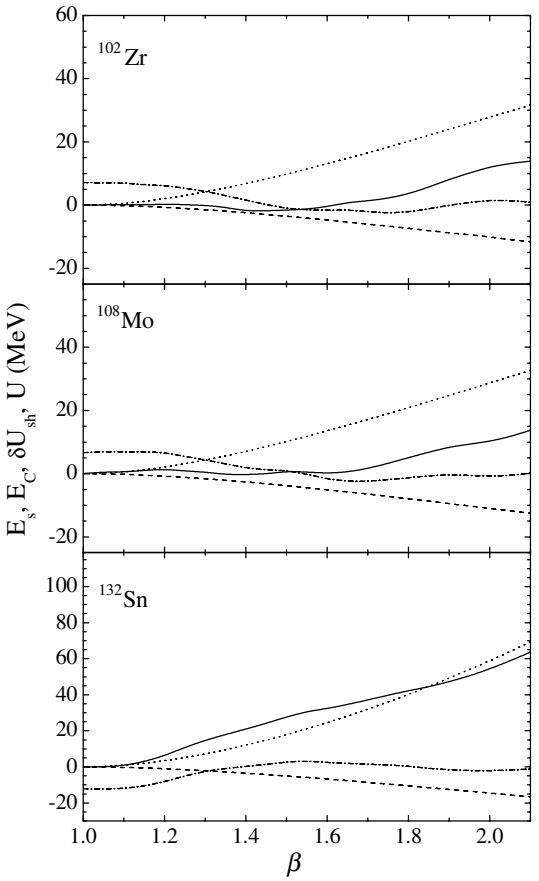

Fig. 1. The dependence of the surface (dotted lines), Coulomb (dashed lines) energies, shell corrections (dot-dashed lines) and total potential energies (solid lines) of ^{102}Zr, ^{108}Mo and ^{132}Sn on the deformation parameter. The surface, Coulomb and total energies are referred to their values for spherical nucleus.

In order to include the dependence of the shell correction on excitation energy E^*, the following phenomenological expression is widely used:

$$\delta U^i_{\rm sh}(A_i, Z_i, \beta_i, E^*) = \delta U^i_{\rm sh}(A_i, Z_i, \beta_i, E^* = 0)\exp[-E^*_i/E_{\rm D}], \qquad (6)$$

where the damping constant $E_{\rm D} = 18.5$ MeV [28]. Since the extraction of excitation energies E^*_i of the fission fragments from the experimental data is only known for few

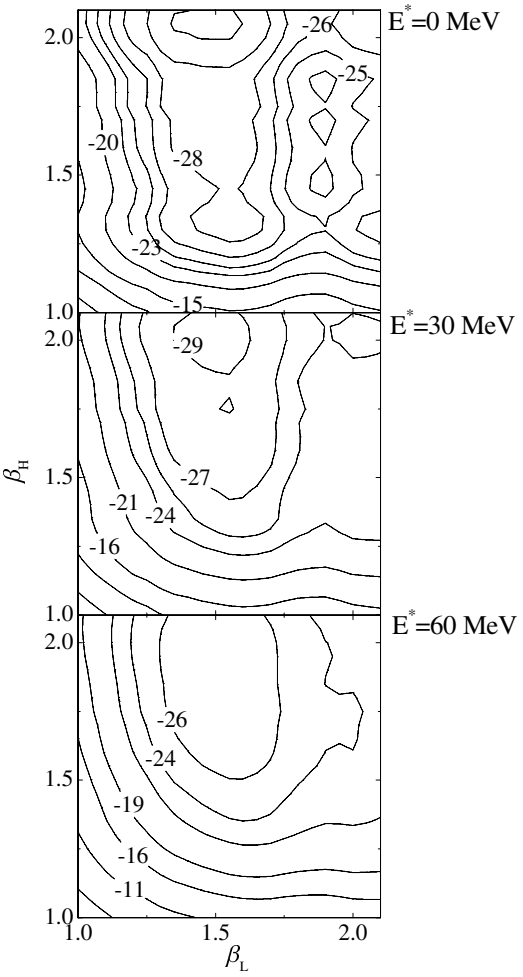

Fig. 2. Potential energies of the scission configuration ($R = R_b(\beta_L, \beta_H)$) as functions of β_L and β_H for the fission $^{234}\mathrm{U} \to {}^{90}\mathrm{Kr} + {}^{144}\mathrm{Ba}$ at the excitation energies $E^* = 0$, 30 and 60 MeV. The potential energy is set zero at $\beta_L = \beta_H = 1$.

splittings [9], we assume for simplicity $E_i^* = A_i E^*/(A_L + A_H)$. We found for the considered excitation energies that our final results are not sensitive to a reasonable variation of E_D within the interval 15–25 MeV as well as to the assumption on the sharing of excitation energy between the fragments. The dependence of the potential energy as a function of β_L and β_H on the excitation energy is shown in fig. 2. While the potential energy surface has few minima for small E^*, the number of minima decreases with increasing E^*. At $E^* = 60$ MeV, the liquid-drop limit is reached. Since in neutron-induced and spontaneous fission the excitation energy of scission configuration does not exceed about 30 MeV, the shell effects play an important role in the formation of the TKE-mass distribution of fission fragments. If the fissioning system reaches the scission configuration, which we assume as a DNS configuration, its probability is distributed in the space of deformation parameters in accordance with the potential energy surface, *i.e.*, the scission occurs with some probability at each β_L and β_H for a fixed mass or charge splitting.

2.3 Discussion of shape parametrization

For the ellipsoid with deformation parameter β, the charge quadrupole Q_2 and hexadecupole Q_4 moments are [18]

$$Q_2 = \frac{2Ze}{5} R_0^2 \frac{\beta^2 - 1}{\beta^{2/3}},$$
$$Q_4 = \frac{9Ze}{70\sqrt{\pi}} R_0^4 \frac{(\beta^2 - 1)^2}{\beta^{4/3}}, \quad (7)$$

where R_0 is the radius of the equivalent spherical nucleus. If one uses the multipole expansion of the nuclear surface $R = R_0(1 - (\beta_2^2 + \beta_4^2)/(4\pi) + \beta_2 Y_{20}(\theta) + \beta_4 Y_{40}(\theta))$ with the parameters of quadrupole (β_2) and hexadecupole (β_4) deformations, Q_2 and Q_4 are calculated as follows [18]:

$$Q_2 \approx \frac{3Ze}{\sqrt{5\pi}} R_0^2 \beta_2 (1 + 0.36\beta_2 + 0.967\beta_4),$$
$$Q_4 \approx \frac{3Ze}{4\pi} R_0^4 (\beta_4 + 0.725\beta_2^2 + 0.983\beta_2\beta_4). \quad (8)$$

Equating the corresponding moments in eq. (7) and eq. (8), one can find the relationship between β_2 and β_4, and β. For example, the ellipsoid with $\beta = 1.2$ has quadrupole and hexadecupole moments corresponding to $\beta_2 = 0.19$ and $\beta_4 = 0.02$. Near the ground states corresponding to small $\beta < 1.3$ the used ellipsoid nuclear shape cannot accommodate higher-even-multipole deformations β_λ ($\lambda \geq 4$). The absolute value of β_4 strongly increases with β. The most probable deformations $\beta_L = 1.7$ and $\beta_H = 1.6$ at scission in the fission of ^{252}Cf into ^{106}Mo and ^{146}Ba with emission of (3–4) neutrons (see sect. 4.1) correspond to $\beta_2 = 0.50$, $\beta_4 = 0.24$ and $\beta_2 = 0.45$, $\beta_4 = 0.17$, respectively, for the multipole expansions of nuclear surfaces. The TKE calculated with these (β_2, β_4)-shapes is about 1 MeV smaller than the TKE calculated with the ellipsoid shapes in the present paper. Since for large β, in which we are mainly interested in the fission accompanied by the neutron evaporation, the higher even multipoles ($\lambda \geq 4$) are effectively in our consideration, the difference between the TKE calculated with other shape parametrizations becomes small. In the present paper we consider also several cases with small β but for the nuclei which are not expected to have the deformations of higher multipoles, for example, ^{126,132}Sn. Therefore, the used ellipsoid shapes are quite suitable for the schematic calculations of fission events considered in the paper and for the analysis of reasons responsible for the fine structures in the TKE-mass distribution. Note that the ellipsoid shapes are consistent with the calculations of δU_sh within the two-center shell model.

While the present model is applicable to the description of fission events which are mainly characterized by quite large deformations of the fragments at scission, it is not yet adopted for the description of the cold fission in which the fragments at scission are nearly their ground states and some of the fragments are expected to be hexadecupole-deformed according to the macroscopic-microscopic calculations [27]. In the cold-fission splitting $^{252}\mathrm{Cf} \to {}^{106}\mathrm{Mo} + {}^{146}\mathrm{Ba}$, $\beta_L \approx 1.4$ ($\beta_2 = 0.361$) and

$$\langle \mathrm{TKE} \rangle (\{A_i, Z_i\}) = \frac{\int \mathrm{TKE}(\{A_i, Z_i, \beta_i\}) \exp[-U(\{A_i, Z_i, \beta_i\}, R_b, E^*)/T] \mathrm{d}\beta_L \mathrm{d}\beta_H}{\int \exp[-U(\{A_i, Z_i, \beta_i\}, R_b, E^*)/T] \mathrm{d}\beta_L \mathrm{d}\beta_H} \quad (11)$$

$\beta_H \approx 1.23$ ($\beta_2 = 0.22$) [27], and the present model overestimates the TKE by 4.5 MeV due to the lack of suitable hexadecupole deformation ($\beta_4 = 0.1$) in the ellipsoid parametrization of ^{146}Ba.

3 Total kinetic energy of fission fragments

At fixed mass and charge splittings $\{A_i, Z_i\}$ the total kinetic energy of the fission fragments is defined as

$$\mathrm{TKE}(\{A_i, Z_i, \beta_i\}) = V_\mathrm{C}(\{A_i, Z_i, \beta_i\}, R_b) + V_\mathrm{N}(\{A_i, Z_i, \beta_i\}, R_b)\,. \quad (9)$$

The excitation energy of the scission configuration is related to the Q-value as follows:

$$E^*(\{A_i, Z_i, \beta_i\}, R_b) = Q - \mathrm{TKE}(\{A_i, Z_i, \beta_i^{\mathrm{gs}}\}) + S - \{U(\{A_i, Z_i, \beta_i\}, R_b, E^*) - U(\{A_i, Z_i, \beta_i^{\mathrm{gs}}\}, R_b, E^*)\}\,, \quad (10)$$

where $S = S_n \approx 8$ MeV is the excitation energy coming from the thermal neutron in the neutron-induced fission. In spontaneous fission S is zero. In photofission S is equal to the energy of gamma quanta. The deformation parameters β_L^{gs} and β_H^{gs} are related to the ground states of the nuclei and calculated for separate nuclei. The difference of the total energy of the excited system with respect to the energy of the system with the nuclei in their ground states consists of the difference of the TKE and of the energy of deformation.

Since the potential energy depends on E^*, the excitation energy is calculated with (10) by using an iteration procedure. First, U is defined with $E^* = 0$ MeV and a new value of E^* is found from (10). Then, with this E^* we calculate the potential energy U which leads to a new value of E^*. As we checked, these two steps supply a nice accuracy for finding E^* because we deal with excitation energies at which the damping of the shell effects is rather small.

In the scission point model within statistical assumption the mean total kinetic energies for fixed $\{A_i, Z_i\}$ are calculated as

see eq. (11) *above.*

Here, the scission configuration is assumed in the thermodynamic equilibrium, with a certain distribution in β_L and β_H. For fixed A_i and Z_i, the excitation energy E^* is defined by the deepest minimum of the potential energy as a function of β_L and β_H with $1 \le \beta_L$, $\beta_H \le 2.1$. The corresponding effective temperature is $T = \sqrt{12E^*/(A_L + A_H)}$. It should be noted that in our model the temperature is not a free parameter as in ref. [1], but obtained from the excitation energy of the internal degrees of freedom.

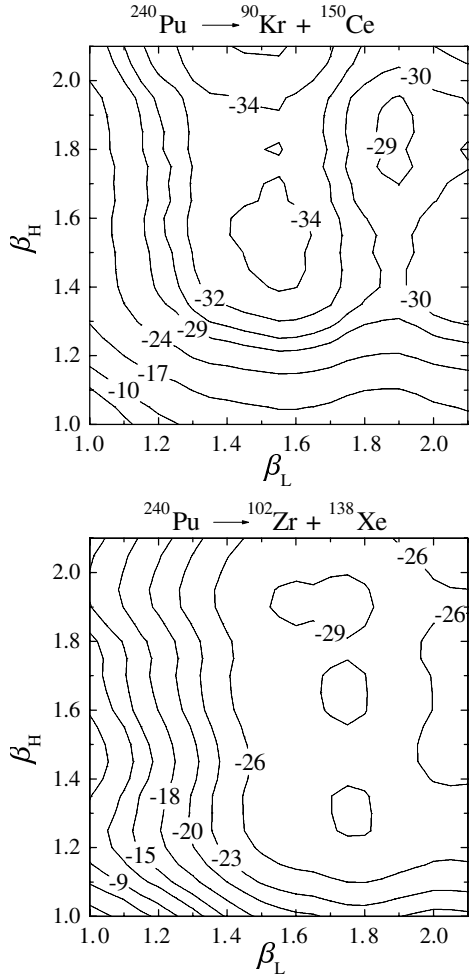

Fig. 3. Potential energies of scission configurations ($R = R_b(\beta_L, \beta_H)$) as functions of β_L and β_H for the indicated neutron-induced fission fragmentations.

In order to avoid cumbersome calculations, we search for $Z_i = Z_i^m$ for fixed A_i at which the potential energy is minimal and, thus, the fission yield for $\{A_i, Z_i\}$ is maximal. The found most probable charge numbers Z_i^m for each A_i are in a good agreement with the experimental data. Indeed, for fixed A_i the distribution of fission fragments in Z_i is very narrow. For the considered excitations of the scission configurations, the TKE is assumed to be approximately: $\langle \mathrm{TKE} \rangle (\{A_i\}) \approx \langle \mathrm{TKE} \rangle (\{A_i, Z_i = Z_i^m\})$. The variance of TKE, $\sigma^2_{\mathrm{TKE}}(\{A_i\}) = \langle [\mathrm{TKE}(\{A_i, Z_i, \beta_i\}) - \langle \mathrm{TKE} \rangle (\{A_i\})]^2 \rangle$, is the result of the same average over β_L and β_H as in (11). Again we assume $\sigma^2_{\mathrm{TKE}}(\{A_i\}) \approx \sigma^2_{\mathrm{TKE}}(\{A_i, Z_i^m\})$.

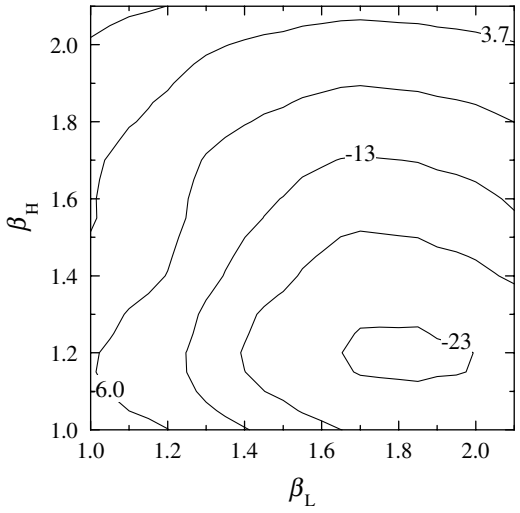

Fig. 4. The same as in fig. 3, but for the neutron-induced fission reaction $^{240}\mathrm{Pu} \rightarrow {}^{106}\mathrm{Mo} + {}^{134}\mathrm{Te}$.

4 Results of calculations and discussion

4.1 Minima of potential energy with respect to β_L and β_H

The potential energies of scission configurations as functions of β_L and β_H are presented in figs. 3–5 for the splittings $^{240}\mathrm{Pu} \rightarrow {}^{90}\mathrm{Kr} + {}^{150}\mathrm{Ce}$, $^{102}\mathrm{Zr} + {}^{138}\mathrm{Xe}$ and $^{106}\mathrm{Mo} + {}^{134}\mathrm{Te}$, $^{252}\mathrm{Cf} \rightarrow {}^{106}\mathrm{Mo} + {}^{146}\mathrm{Ba}$ and $^{258}\mathrm{Fm} \rightarrow {}^{126}\mathrm{Sn} + {}^{132}\mathrm{Sn}$. The calculations are shown for the parameters of deformations smaller than 2.1 up to which the used shape parametrization is suitable. One can see several minima in the potential U. The number of minima becomes smaller for more symmetric splittings. For example, in the case of $^{252}\mathrm{Cf} \rightarrow {}^{106}\mathrm{Mo} + {}^{146}\mathrm{Ba}$ there is only one minimum in the considered interval of β_L and β_H (fig. 5). With the used shape parametrization one obtains a second minimum at larger $\beta_H = 2.2$ as well. However, the DNS, which is already unstable with respect to the decay for smaller β_H, reaches this minimum with very small probability. Perhaps this explains the negligible role of the second mode in the fission of $^{252}\mathrm{Cf}$ which corresponds to small TKE [9]. In the fission splitting $^{240}\mathrm{Pu} \rightarrow {}^{102}\mathrm{Zr} + {}^{138}\mathrm{Xe}$, the potential has three minima at $\beta_L \approx 1.75$ which are close to each other.

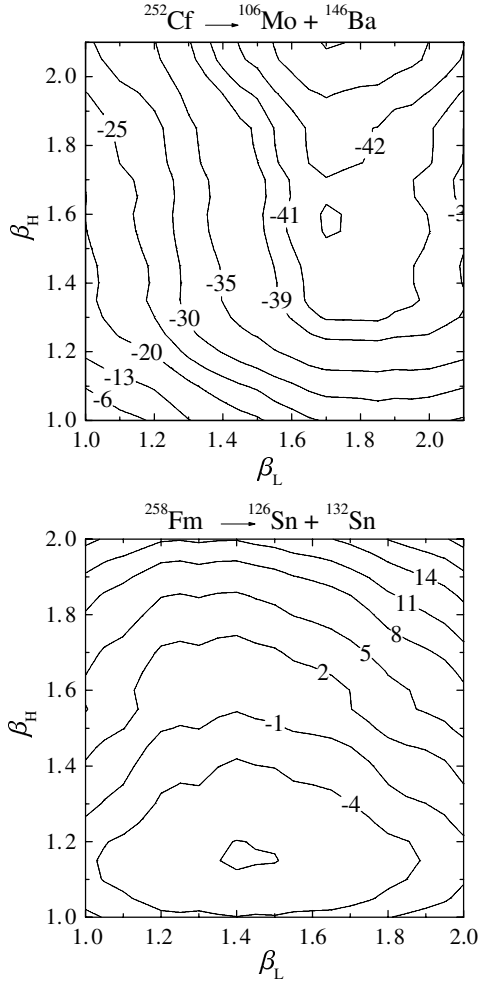

Fig. 5. The same as in fig. 3, but for the indicated spontaneous fission reactions.

4.2 Fine structure of the TKE-mass distribution

Besides β_L and β_H, the DNSs associated with the scission configurations are characterized by the mass and charge asymmetry coordinates supplying different mass and charge fragmentations in fission. If we consider the DNS potential energy as a function of A_L (or A_H), β_L and β_H, the potential energy surface depends on three coordinates. In the previous subsection we showed that there are several minima of the DNS potential energy as a function of β_L and β_H for fixed A_L and A_H. The deformations β_L and β_H of the fragments at these minima have almost the same values for neighboring A_L. Therefore, in the three-dimensional space (β_L, β_H, A_L) the minima of the potential energy with respect to β_L and β_H are aligned with several lines almost perpendicular to the plane (β_L, β_H). Due to the existence of these minima and the relatively enhanced yield of fission in R from them, the formation of the fine structures of the TKE-mass distribution of the fission fragments is possible. Since the minima in β_L and β_H are rather shallow and appear also in the neighboring charge splittings at fixed A_L, one would not observe well-distinguished peaks in the TKE-mass distribution in the experiment. If only one minimum existed with respect to β_L and β_H at each A_L on the potential energy surface, the TKE-mass distribution of the fission fragments would have no the fine structures.

We calculated the TKE as a function of A_L in the fission of $^{234}\mathrm{U}$ at each minimum in β_L and β_H and show the result as a function of A_L in fig. 6. For each A_L, we have points which correspond to pairs of fragments with the values of β_L and β_H at the minima in the considered interval of deformation parameters. One can see from the connections of the calculated points by straight lines

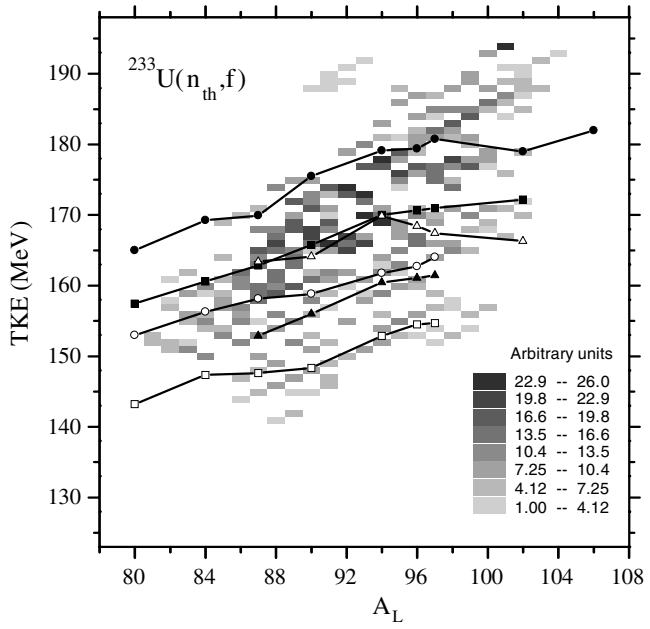

Fig. 6. Comparison of calculated and experimental fine structures in the TKE-mass distribution of neutron-induced fission of ^{234}U. At each A_L, the solid and open symbols denote the TKE of scission configurations at the minima of the potential energy as functions of β_L and β_H. Solid circles correspond to configurations with smallest β_L and β_H among all minima. Open squares correspond to configurations with largest β_L and β_H among all minima (β_L, $\beta_H \leq 2.1$). TKEs of scission configurations with smallest β_L-largest β_H, smallest β_L-medium β_H, largest β_L-medium β_H and largest β_L-smallest β_H are shown by open circles, open triangles, solid triangles and solid squares, respectively. The lines are given to guide the eye. The experimentally observed fine structures [14] are presented in arbitrary units.

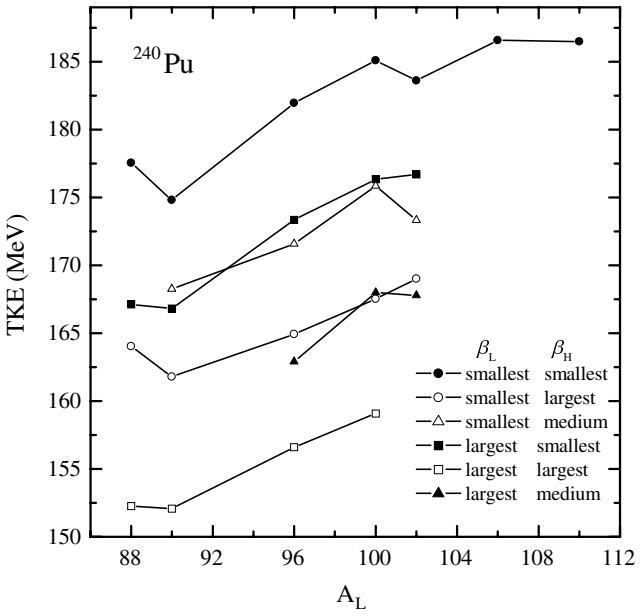

Fig. 7. The same as in fig. 6, but for the calculated fine structures in neutron-induced fission of ^{240}Pu.

Table 1. Comparison of experimental (exp) [7,12,13] and calculated (th) mean TKE of pairs of fission fragments.

Fragmentation	$\langle \mathrm{TKE} \rangle_{\mathrm{exp}}$ (MeV)	$\langle \mathrm{TKE} \rangle_{\mathrm{th}}$ (MeV)
$^{232}\mathrm{Th} \rightarrow {}^{98}\mathrm{Sr} + {}^{134}\mathrm{Te}$	168	174
$^{232}\mathrm{Th} \rightarrow {}^{88}\mathrm{Se} + {}^{144}\mathrm{Ba}$	158	153.5
$^{232}\mathrm{Th} \rightarrow {}^{114}\mathrm{Ru} + {}^{118}\mathrm{Pd}$	153	159
$^{250}\mathrm{Cf} \rightarrow {}^{74}\mathrm{Zn} + {}^{176}\mathrm{Er}$	159	164.5
$^{250}\mathrm{Cf} \rightarrow {}^{80}\mathrm{Ge} + {}^{170}\mathrm{Dy}$	164	169
$^{250}\mathrm{Cf} \rightarrow {}^{88}\mathrm{Kr} + {}^{162}\mathrm{Sm}$	170.5	177.5
$^{252}\mathrm{Cf} \rightarrow {}^{124}\mathrm{Cd} + {}^{128}\mathrm{Sn}$	192	198
$^{252}\mathrm{Cf} \rightarrow {}^{74}\mathrm{Ni} + {}^{178}\mathrm{Yb}$		159
$^{258}\mathrm{Fm} \rightarrow {}^{126}\mathrm{Sn} + {}^{132}\mathrm{Sn}$	230	229
$^{258}\mathrm{Fm} \rightarrow {}^{126}\mathrm{Cd} + {}^{132}\mathrm{Te}$	205	198
$^{258}\mathrm{No} \rightarrow {}^{126}\mathrm{Cd} + {}^{132}\mathrm{Xe}$	204	200.5

in fig. 6 that on the plane (TKE, A_L) several curves are formed along which the yield of fission products should be relatively enhanced. These curves correlate with the experimental enlarged yields [14] which produce fine structures of the TKE-mass distribution. These structures are different from those produced by the odd-even effect. Indeed, the method for analysing the fine structure in the experimental data is based on the specific subtraction of a smooth distribution from the measured one [14]. The present calculation maintains the correlation with the experiment but we cannot conclude whether the presence of the potential energy minima in the (β_L, β_H)-plane is the only reason for the observed fine structure. Other effects like the formation of complicated cluster configurations [15] may contribute to the fine structure as well.

In fig. 7 we predict the fine structures in the TKE-mass distribution of fission fragments of ^{240}Pu. These structures are more complicated for $88 \leq A_L \leq 102$. For $A_L \geq 104$, there is only one minimum of the potential energy as a function of β_L and β_H at fixed A_L.

4.3 Mean TKE, variance of TKE and relative yields of fission fragments

The experimentally determined fission fragments are those after neutron evaporation. The calculated quantities, however, are the primary mass and energy distributions of the fission fragments before prompt neutron emission. In order to reconstruct the pre-neutron yield, a Monte Carlo simulation is used [3]. The emission of one neutron changes the kinetic energy by about 1 MeV [7]. Since for ^{234}U, ^{240}Pu and ^{250}Cf the pre-neutron yields are not presented in refs. [2,5,7], we added the difference between the pre- and post-neutron TKE at the same A_L, presented for ^{236}U fission in ref. [3], to the measured post-neutron TKE. Thus, the TKEs of primary fission fragments are 1–3 MeV larger than those after neutron emission and these values are compared with our calculated results.

The success of our model in describing $\langle \mathrm{TKE} \rangle$ is demonstrated in fig. 8 for the neutron-induced fission of

Table 2. Comparison of experimental (exp) [9] and calculated (th) mean TKE, variances of TKE and relative yields (Y) for different pairs of fragments in spontaneous fission of ^{252}Cf.

Fragmentation	$\langle \mathrm{TKE} \rangle_{\mathrm{exp}}$ (MeV)	$\sigma^2_{\langle \mathrm{TKE} \rangle_{\mathrm{th}}}$ (MeV^2)	$\langle \mathrm{TKE} \rangle_{\mathrm{th}}$ (MeV)	$\sigma^2_{\langle \mathrm{TKE} \rangle_{\mathrm{exp}}}$ (MeV^2)	Y_{exp}	Y_{th}
^{102}Zr + ^{150}Ce	183.3(3)	106	179.3	99(9)	0.21	0.18
^{106}Mo + ^{146}Ba	189.3(1)	89	190	89.5(4)	0.44	0.54
^{112}Ru + ^{140}Xe	193.3(3)	90	194.8	95(7)	0.25	0.21
^{118}Pd + ^{134}Te	200	65	198		0.1	0.06

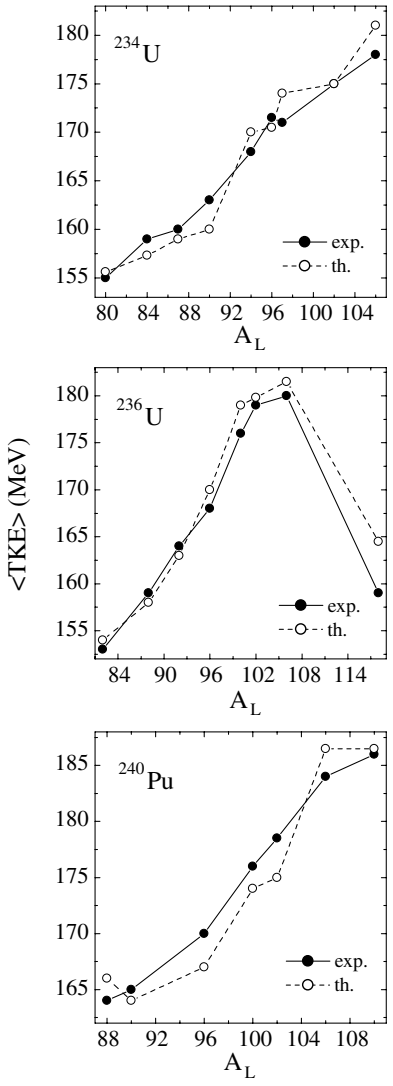

Fig. 8. Calculated and experimental [2–5] mean $\langle \mathrm{TKE} \rangle (\{A_i\})$ as a function of A_L for neutron-induced fission of ^{234,236}U and ^{240}Pu. The shown points are connected by lines to guide the eye. For fixed A_L, the most probable charge splitting was found by minimization of the total energy with respect to Z_L.

^{234,236}U and ^{240}Pu. The agreement of the calculated results and the available experimental data is within 5 MeV. A comparison of calculated and experimental values of $\langle \mathrm{TKE} \rangle (\{A_i, Z_i\})$ is listed in tables 1 and 2 for photofission of ^{232}Th, neutron-induced fission of ^{250}Cf, and spontaneous fission of ^{252}Cf, ^{256}No and ^{258}Fm. The agreement of theory with the experiment is quite good. For ^{252}Cf spontaneous fission, the variances of TKE listed in table 2 are well described. The experimental uncertainties are larger for rare asymmetric fission events. For example, ref. [7] gives $\langle \mathrm{TKE} \rangle \approx 153$ MeV and ref. [29] gives $\langle \mathrm{TKE} \rangle \approx 159$ MeV for the same fragmentation $A_L/A_H = 74/176$ in the fission of ^{250}Cf. A larger deviation of the calculated $\langle \mathrm{TKE} \rangle$ from the experimental data for asymmetric fission splitting could also indicate the necessity of a dynamical treatment of the decay out of the asymmetric DNS instead of the statistical approach used in the present paper. The same fission mass splitting of ^{258}Fm with different Z_L leads to quite different values of $\langle \mathrm{TKE} \rangle$ that is possible to check in the experiment.

In order to calculate the relative yields within the statistical treatment [1], we use the potential energies of each configuration at the corresponding deepest minimum in the potential energy surface in the (β_L, β_H)-plane. In table 2 the calculated and experimental relative yields Y are in a good agreement for the indicated fragments of spontaneous fission of ^{252}Cf. The calculated ratio between the yields of pairs ^{106}Mo+^{146}Ba and ^{74}Ni+^{178}Yb is about $1 : 10^{-5}$, where the splitting ^{106}Mo+^{146}Ba has the maximal yield of fission fragments of ^{252}Cf. For the fission of ^{240}Pu, we obtained 0.37 : 0.63 for the ratio of mass yield of the fission mode ST1 with $A_H = 134$ to the one of the fission mode ST2 with $A_H = 140$ that is consistent with the experimental ratio 0.264 : 0.736 [6]. However, the experimental ratio 200 : 1 [4] between the yields of asymmetric and symmetric fissions of ^{236}U is not reproduced in our calculation which gives a ratio 200 : 7. As was mentioned in ref. [1], this difference could be created by the uncertainties in the calculation of shell corrections. The shell correction method is not expected to be more accurate than 0.5–1 MeV. This could create a quantitative disagreement in some cases.

For the calculations of $\langle \mathrm{TKE} \rangle$ and σ^2_{TKE}, we assumed the thermodynamic equilibrium in the DNS with effective temperature T. The partition of the excitation energy $E^*_L/E^*_H = A_L/A_H$ between the fragments at scission point is used to take into account the damping of the shell correction with excitation. The excitation energies of the fragments at scission and at the asymptotic differ by the deformation energies of the fragments at scission. The total excitation energy of the scission configuration is small when one of the fragments is magic nucleus. A sawtooth structure for the neutrons emitted as a function of fragment mass is reproduced well in the scission point models, for example, in ref. [1]. We checked that for the

Table 3. Comparison of mean TKE calculated at different values of E_L^*/E_H^* for the indicated fragmentations in spontaneous fission of ^{252}Cf. The values of E_L^*/E_H^* taken from ref. [9] were obtained with unfolding procedure from the experimental data.

Fragmentation	E_L^*/E_H^*	$\langle \mathrm{TKE} \rangle_{\mathrm{th}}$ (MeV)
^{102}Zr + ^{150}Ce	$A_L/A_H = 0.68$	179.3
	1	178.9
^{105}Mo + ^{147}Ba	$A_L/A_H = 0.71$	190.3
	1	190.3
	0.2 [9]	190.3
^{106}Mo + ^{146}Ba	$A_L/A_H = 0.73$	190
	1	190
	1.38 [9]	192.5
^{107}Mo + ^{145}Ba	$A_L/A_H = 0.74$	190.7
	1	191
	0.64 [9]	190.6

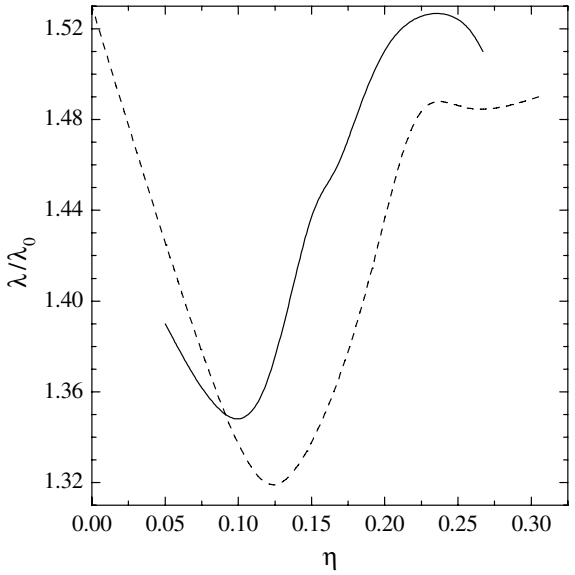

Fig. 9. The ratio of the length λ of the fissioning system at $R = R_b$ with deformations β_L and β_H corresponding to the deepest minimum on the potential energy surface to the length λ_0 of the same system at $\beta_L = \beta_H = 1$ as a function of the mass asymmetry for ^{236}U (dashed line) and ^{240}Pu (solid line).

spontaneous fission, neutron-induced fission and photofission our results are not crucial to the partition of the excitation energy between the fragments at scission point. In table 3 we illustrate this for several splittings of ^{252}Cf. If we set $E_{\mathrm{D}} \to \infty$ in (6) (no damping of the shell correction), we obtain $\langle \mathrm{TKE} \rangle$ = 177.4, 193.4, 191.5 and 193.5 MeV for the fissions $^{252}\mathrm{Cf} \to {}^{102}\mathrm{Zr} + {}^{150}\mathrm{Ce}$, $^{105}\mathrm{Mo} + {}^{147}\mathrm{Ba}$, $^{106}\mathrm{Mo} + {}^{146}\mathrm{Ba}$ and $^{107}\mathrm{Mo} + {}^{145}\mathrm{Ba}$, respectively. Therefore, the dependence of our results on the damping of the shell corrections and the partition of the excitation between the fragments is within the inaccuracy of the calculations and experimental measurements. In the splittings $^{105}\mathrm{Mo} + {}^{147}\mathrm{Ba}$ and $^{107}\mathrm{Mo} + {}^{145}\mathrm{Ba}$ of ^{252}Cf the potential energies at scissions are about 2.5 MeV larger than the potential energy at scission for the splitting $^{106}\mathrm{Mo} + {}^{146}\mathrm{Ba}$. Therefore, $^{106}\mathrm{Mo} + {}^{146}\mathrm{Ba}$ is the most probable fission splitting of ^{252}Cf for $Z_L = 42$ and $Z_H = 56$ [9]. From the example presented in table 3 one can see that the value of $\langle \mathrm{TKE} \rangle$ weakly depends on $A_L\,(A_H)$ at fixed $Z_L\,(Z_H)$. Therefore, for each $Z_L\,(Z_H)$ the experimental TKE averaged over various mass fragmentations can be successfully compared with $\langle \mathrm{TKE} \rangle$ calculated for the most probable $A_L\,(A_H)$.

Figure 9 shows the ratio of the length of the fissioning system at $R = R_b$ with deformations β_L and β_H corresponding to the deepest minimum of the potential energy to the length of the same system with $\beta_L = \beta_H = 1$ as a function of the mass asymmetry $\eta = (A_H - A_L)/(A_L + A_H)$ for the systems ^{236}U and ^{240}Pu. The fission fragments with the largest yield have smaller relative deformations. Here, we find $\eta = 0.13$ ($A_H = 134$, $A_L = 102$) for ^{236}U and $\eta = 0.11$ ($A_H = 136$, $A_L = 106$) for ^{240}Pu, where this ratio is minimal, in comparison with the largest experimental yields for $\eta = 0.15$–0.19 [3] and 0.13 [5], respectively.

5 Summary

Within an improved scission point model we calculated the mean TKE of the fission fragments of ^{232}Th, ^{234,236}U, ^{240}Pu, ^{250,252}Cf, ^{256}No and ^{258}Fm. In the most cases the agreement with the experimental data is quite good. In comparison to ref. [1], our method allows us to define strictly the scission configuration for each fission splitting and each set of deformation parameters and excitation energies. We can describe the variance of TKE and relative yield of each mass (charge) splitting. For fixed A_L, the fragmentations are relatively enhanced from the minima of the potential energy surface as a function of the deformation parameters. This creates the fine structures in the TKE-mass distribution of fission fragments. Although the experimentally observed fine structures are rather complicated and are probably not produced by only the deformation effects considered here, the correlation of the calculated and experimental structures supports the possible explanation of the observed phenomena by the deformation of the fragments.

We thank Prof. Yu.V. Pyatkov and Dr V.G. Tishchenko for discussions of the fine structures. We thank Prof. G.M. Ter-Akopian for fruitful discussion of the results on spontaneous fission of ^{252}Cf. A.V.A. thanks the DAAD (Bonn) for the support. This work was supported by Volkswagen-Stiftung (Hannover), DFG (Bonn), RFBR (Moscow) and STCU (Uzb-45).

References

1. B.D. Wilkins, E.P. Steinberg, R.R. Chasman, Phys. Rev. C **14**, 1832 (1976).
2. U. Quade *et al.*, Nucl. Phys. A **487**, 1 (1988).
3. W. Lang, H.G. Clerc, H. Wohlfarth, H. Schrader, K.H. Schmidt, Nucl. Phys. A **345**, 34 (1980).
4. F.J. Hambsch, H.H. Knitter, C. Budtz-Jorgensen, J.P. Theobald, Nucl. Phys. A **491**, 56 (1989).
5. C. Schmitt *et al.*, Nucl. Phys. A **430**, 21 (1984).

6. L. Dematte, C. Wagemans, R. Barthelemy, P.D'hondt, A. Deruytter, Nucl. Phys. A **617**, 331 (1997).
7. R. Hentzschel, H.R. Faust, H.O. Denschlag, B.D. Wilkins, J. Gindler, Nucl. Phys. A **571**, 427 (1994).
8. M. Djebra *et al.*, Nucl. Phys. A **496**, 346 (1989).
9. G.M. Ter-Akopian *et al.*, Phys. Rev. C **55**, 1146 (1997); G.M. Ter-Akopian, private communication.
10. C. Budtz-Jorgensen, H.H. Knitter, Nucl. Phys. A **490**, 307 (1988); **491**, 56 (1989).
11. G. Barreau *et al.*, Nucl. Phys. A **432**, 411 (1985).
12. M. Piessens, E. Jacobs, S. Pomme, D. de Frenne, Nucl. Phys. A **556**, 88 (1993).
13. E.K. Hulet *et al.*, Phys. Rev. C **40**, 770 (1989).
14. Yu.V. Pyatkov, V.G. Tishchenko, V.V. Pashkevich, V.A. Maslov, D.V. Kamanin, I.V. Kljuev, W.H. Trzaska, Nucl. Instrum. Methods A **488**, 381 (2002).
15. Yu.V. Pyatkov, G.G. Adamian, N.V. Antonenko, V.G. Tishchenko, Nucl. Phys. A **611**, 355 (1996).
16. J. Maruhn, W. Greiner, Phys. Rev. Lett. **32**, 548 (1974).
17. A. Sandulescu, A. Florescu, W. Greiner, J. Phys. G **15**, 1851 (1989).
18. R.W. Hasse, W.D. Myers, *Geometrical Relationships of Macroscopic Nuclear Physics* (Springer-Verlag, Berlin, 1988).
19. G.G. Adamian *et al.*, Int. J. Mod. Phys. E **5**, 191 (1996).
20. T.M. Shneidman, G.G. Adamian, N.V. Antonenko, S.P. Ivanova, R.V. Jolos, W. Scheid, Phys. Rev. C **65**, 064302 (2002).
21. W. Greiner, J.Y. Park, W. Scheid, *Nuclear Molecules* (World Scientific, Singapore, 1995).
22. R.W. Hasse, Ann. Phys. (NY) **68**, 377 (1971).
23. V.M. Strutinsky, Sov. Phys. JETP **18**, 1298 (1964).
24. P. Möller, R. Nix, At. Data Nucl. Data Tables **39**, 213 (1988); Nucl. Phys. A **361**, 117 (1980); LANL Preprint LA-UR-86-3983 1986.
25. A. Bohr, B. Mottelson, *Nuclear Structure*, Vol. **2** (W.A. Benjamin, New York, Amsterdam, 1974).
26. S. Raman, C.W. Nestor, P. Tikkanen, At. Data Nucl. Data Tables **78**, 1 (2001).
27. P. Möller, R. Nix, W.D. Myers, W.J. Swiatecki, At. Data Nucl. Data Tables **59**, 185 (1995).
28. A. Ignatyuk, *Statistical Properties of Excited Atomic Nuclei* (Energoatomizdat, Moscow, 1983).
29. U. Brosa, S. Grossman, A. Müller, Phys. Rep. **197**, 167 (1990).